Stenoparib, an inhibitor of cellular poly (ADP-ribose) polymerase (PARP), blocks replication of the SARS-CoV-2 human coronavirus *in vitro*.

Nathan E. Stone[a], Sierra A. Jaramillo[a], Ashley N. Jones[a], Adam J. Vazquez[a], Madison Martz[a], Lora M. Versluis[ab], Marlee O. Raniere[ab]., Haley E. Nunnally[a], Katherine E. Zarn[a], Roxanne Nottingham[a], Jason W. Sahl[ab], David M. Wagner[ab], Steen Knudsen[c], Erik W. Settles[ab], Paul S. Keim[ab], Christopher T. French[ab]#.

[a]Pathogen and Microbiome Institute, Northern Arizona University, Flagstaff, AZ 86011-4073

[b]Department of Biological Sciences, Northern Arizona University, Flagstaff, AZ 86011-5640

[c]Allarity Therapeutics, DK-2970 Hørsholm, Denmark

Running Head: Stenoparib inhibits SARS-CoV-2 *in vitro* (character limit 54 with spaces)

#Address correspondence to Christopher T. French, ctfrench@nau.edu

Abstract

By late 2020, the coronavirus disease (COVID-19) pandemic, caused by SARS-CoV-2 has caused tens of millions of infections and over 1 million deaths worldwide. A protective vaccine and more effective therapeutics are urgently needed. We evaluated a new PARP inhibitor, stenoparib, for which was recently advanced to Stage II clinical trials for treatment of ovarian cancer. This is an initial report on the activity of stenoparib against human respiratory coronaviruses, including SARS-CoV-2, *in vitro*. Stenoparib exhibits dose-dependent suppression of SARS-CoV-2 multiplication and spread in Vero E6 monkey kidney and Calu-3 human lung

adenocarcinoma cells. Stenoparib was also strongly inhibitory to multiplication of the HCoV-NL63 human seasonal respiratory coronavirus. Compared to remdesivir, which inhibits the viral replicon subsequent to cell entry, stenoparib is inhibitory to virus entry and post-entry processes as determined by time-of-addition (TOA) experiments. Moreover, a 10 μM dosage of stenoparib, which is far below its 25.5 μM half-maximally effective concentration (EC_{50}), when combined with 0.5 μM remdesivir suppressed coronavirus growth by 90.7%, indicating a potentially synergistic effect for this drug combination. Thus, stenoparib as a standalone or as a component of combinatorial therapy with remdesivir may be a valuable addition to the arsenal against COVID-19.

36 **Importance**

New therapeutics are urgently needed in the fight against COVID-19. Repurposing drugs that are
38 either already approved for human use or are in advanced stages of the approval process can facilitate more rapid advances toward this goal. The PARP inhibitor stenoparib may be such a
40 drug, as it is currently in Stage II clinical trials for the treatment of ovarian cancer and its safety and dosage in humans has already been established. Our results indicate that stenoparib
42 possesses strong antiviral activity against SARS-CoV-2 and other coronaviruses *in vitro.* This activity appears to be based on multiple modes of action, where both pre-entry and post-entry
44 viral replication processes are impeded. This may provide a therapeutic advantage over many current options that have a narrower target range. *Moreover, our results suggest that stenoparib*
46 *and remdesivir may be an especially potent combination against coronavirus infection.*

48

Introduction

50 The novel SARS-CoV-2 coronavirus emerged from Wuhan, China in late 2019, and rapidly spanned the globe in a devastating pandemic (1). The disease, COVID-19, compromises
52 the upper and lower respiratory systems and may affect all people (2). Although in many cases COVID-19 symptoms may be mild, some patients present with pulmonary distress leading to
54 severe lung damage, and treatment options are limited (1, 3-5). Mortality estimates range from 0.5% to more than 5% (6). According to the Johns Hopkins COVID Resource Center (7), as of
56 Nov. 10, 2020, over 10 million infections and more than 240,000 deaths have occurred due to COVID-19 in the USA alone, and the pandemic continues (8). A protective vaccine may
58 eventually be available (1, 2), but unless sufficient herd immunity can be achieved, COVID-19 has the potential to cause morbidity and mortality for years to come. Without a protective
60 vaccine, COVID-19 has largely been controlled through non-pharmaceutical public health measures such as quarantine, social isolation, and the use of personal protective equipment.
62 Clearly, more efficacious treatments are urgently needed.

Individuals who contract COVID-19 are most commonly infected by person-to-person
64 transmission, where inhaled droplets containing infectious virions are seeded into the respiratory tract (1). The virions bind to respiratory epithelium via the affinity of the virus spike (S) complex
66 to the angiotensin converting enzyme 2 (ACE2) receptor (9). A cellular serine protease TMPRSS2 plays a pivotal role in S protein priming (10), which in turn facilitates fusion between
68 the viral and cellular plasma membranes and internalization of the virus-receptor complex by endocytosis. Subsequently, the virus is uncoated and releases its single-stranded RNA genome,
70 which is processed, translated, and replicated in the host cytosol. Copies of the viral genome are packaged into bilayer membrane envelopes, and these new infectious virions are exported from

72 the cell (11, 12). SARS-CoV-2 has a lifecycle typical of other coronaviruses, including the highly virulent SARS-CoV, the cause of Severe Acquired Respiratory Syndrome (SARS) (9).
74 Conservation of key steps in the coronavirus viral lifecycles potentially constitutes an 'Achilles Heel' that is broadly susceptible to therapeutic intervention across species.

76 Antiviral therapeutics impede interactions between the virus and the host cell. Potential targets include the virus binding to the cellular receptor, viral entry or virus-host membrane
78 fusion, viral transcription, translation, replication and export. (1). Stenoparib is an investigational, orally-available small molecule that inhibits poly (ADP- ribose) polymerase
80 (PARP), a key enzyme in DNA repair (13). Stenoparib is unique in that it has dual inhibitory activity against the PARP 1/2 and tankyrase 1/2 enzymes, which are important regulators of the
82 canonical Wnt/β-catenin checkpoint that is often dysregulated in metastatic breast cancer (14). Until August 2020, stenoparib was known as "2X-121" and previously as "E7449". Recently,
84 another PARP inhibitor mefuparib (CVL218) was shown to inhibit SARS-CoV-2 *in vitro*. CVL218 suppressed SARS-CoV-2 infection in Vero E6 African Green Monkey cells (15). As
86 implied by molecular modeling studies, CVL218 and other PARP inhibitors may block viral replication by interfering the viral nucleocapsid (N) protein binding to its RNA template (15).

88 The practice of repurposing existing drugs as treatments for new indications has advantages over developing an entirely new drug (16, 17). There are numerous examples of
90 repurposed drugs in use, including zidovudine, which was repurposed from the treatment of cancer to treat HIV/AIDS; the epilepsy drug topiramate, which is used to treat obesity; aspirin
92 for analgesia and the prevention of colorectal cancer; and others (16). With repurposing, the risk of failure is lower compared to developing a new drug because safety trials have already been
94 completed and the *in vivo* pharmacokinetics have been characterized; thus, cost and time of drug

development are reduced. Moreover, the repurposing endeavor itself may reveal new disease
96 targets and pathways. Altogether, reproposing can produce more rapid and efficient returns (16,
18). Stenoparib is currently in Phase II clinical trials for the treatment of ovarian cancer (14).
98 Based on the recent promising results of the PARP inhibitor CVL218 against SARS-CoV-2 *in vitro* (15), we evaluated the activity of stenoparib against SARS-CoV-2.
100

102 **Results**

Stenoparib inhibits the replication of SARS-CoV-2 in Vero E6 cells. Based on the
104 reported antiviral activity of other PARP inhibitors on SARS-CoV-2 *in vitro* (15) we aimed to
determine whether stenoparib was inhibitory toward the SARS-CoV-2 virus. Stenoparib was
106 prepared as a solution in dimethylsulfoxide (DMSO) and used to treat Vero E6 cells infected
with SARS-CoV-2 (USA-WA1/2020). Vero E6 is a common cell platform for propagating
108 coronaviruses, including SARS-CoV-2 and SARS-CoV (19). At 48 hours (h) after infection,
RNA was isolated from cell supernatants, and viral copy number was estimated by reverse-
110 transcription quantitative real-time polymerase chain reaction (RT-qPCR). Viral RNA
measurements were compared to untreated cell controls, and to cells treated with a cocktail of
112 camostat mesylate and E64d (C/E), which are protease inhibitors that impede processing of the
virus spike protein and interfere with entry into the cell (10, 20). In parallel, we assessed the
114 effects of stenoparib on Vero E6 cells using the lactate dehydrogenase release assay, which
indicates cytotoxicity due to cell lysis. As shown in Fig. 1, stenoparib demonstrated dose-
116 dependent activity against SARS-CoV-2 at concentrations up to 30 μM with negligible
cytotoxicity. The significant 63.2% reduction in viral load following stenoparib treatment
118 ($t=8.608$, $P=0.0010$) is comparable to the results reported for CVL218 (35.2-99.7% inhibition) at
comparable concentrations (15).

120 At concentrations higher than 30 μM, and timepoints exceeding 48 h, stenoparib
displayed marked cytotoxicity to Vero E6 cells (Fig. 2A), which limited our capacity to
122 comprehensively test the activity of the drug. We used a stenoparib response software predictor
to pre-assess the susceptibility of human tumor cells based on the quantitative activity of 414
124 genes (21). When applied to human cell lines used with SARS-CoV-2 (22), the algorithm

predicted that LLC-MK2 cells would be less sensitive to stenoparib toxicity than Vero E6 cells.
126 The cell line Calu-3, originally isolated from the pleural effusion of a patient with lung adenocarcinoma (23), was predicted to be even more resistant than LLC-MK2. This was
128 experimentally verified for Calu-3 cells with stenoparib concentrations up to 60 μM, and exposure for up to 120 h, with no elevation in cytotoxicity (t=8.237, P=0.0144) (Fig. 2B).

130 **Calu-3 lung epithelial cells as a platform for SARS-CoV-2.** Since Calu-3 cells were more resistant to the toxic effects of stenoparib than Vero E6 cells, we utilized Calu-3 cells to
132 test the effectiveness of higher doses than were previously achievable with Vero E6. The viral plaque assay comprehensively assesses inhibitors on the viral intracellular lifecycle, from virus
134 entry, to multiplication, and cell to cell spread. Plaques result from cell damage and death following infection, appearing as empty regions or "dead zones" in the cell monolayer (24).
136 Fresh media containing 2% FBS, with or without stenoparib or C/E control inhibitors, was applied to confluent monolayers of Calu-3 cells, which were then infected with SARS-CoV-2 for
138 1 h. At this time the infection media was removed, and the cells were overlaid with a semisolid matrix consisting of cell growth medium in 1.2% low melting temperature agarose, with or
140 without stenoparib or control inhibitors. At 120 h post infection, cells were fixed with paraformaldehyde, stained with crystal violet, and the number of plaques were visually counted.
142 As shown in Fig. 3A (see also Fig. S1), treatment with 30 μM stenoparib resulted in a 30.6% reduction of plaque forming units (PFUs) per well compared to infected, untreated cells (t=3.054,
144 P=0.0379). Using a higher dose of 60 μM stenoparib, we observed near complete inhibition of plaque formation (94.0%; t=10.24, P=0.0005) with no significant cytotoxicity (t=0.446,
146 P=0.6992), approaching the effect of the C/E control inhibitor (Fig. S1). These observations are mirrored by the results from RT-qPCR, which showed 80.6% reduction of viral copy number

148 with 60 μM stenoparib (P<0.0001). These observations affirm the prediction that Calu-3 cells are more resistant to the effects of stenoparib than Vero E6 cells and are suitable hosts for SARS-

150 CoV-2 *in vitro*. It is interesting to speculate that Calu-3 cells may exhibit a degree of resistance to conditions that can be rapidly toxic in other, more rapidly dividing cell lines, which warrants

152 further exploration. Indeed, the *in vitro* doubling time of Calu-3 cells (>60 h) was notably slower than either the Vero E6 (~24 h) or the LLC-MK2 (~36 h) cell lines.

154 **The NL63 virus as a surrogate *in vitro* model.** In addition to SARS-CoV-2, several other human coronaviruses, including SARS-CoV, interact with human cells via the ACE2

156 receptor, and multiply intracellularly using similar pathways (9). This group includes the respiratory coronavirus HCoV-NL63 (or just 'NL63'), which is a cause of the seasonal colds in

158 humans. While symptoms are generally mild, NL63 infections can be serious in infants and immunocompromised individuals (25-27). Based on its relatedness to SARS-CoV-2, and to

160 establish a surrogate system for use in Biosafety Level-2 (BSL-2) instead of BSL-3 laboratory conditions, we evaluated NL63 for testing the effects of stenoparib.

162 The NL63 virus (NR-470) was propagated in LLC-MK2 Rhesus macaque kidney cells (28). Viral replication levels were assessed by plaque assay and RT-qPCR as performed for

164 SARS-CoV-2. Controls were infected/untreated cells, and infected cells treated with the C/E inhibitor cocktail. Overall, the effects of stenoparib on NL63 corroborated the results of our

166 experiments with SARS-CoV-2. Treatment resulted in a dose-dependent decrease in virus replication, achieving an 69.3% and 95.8% reduction of plaquing efficiency and viral copy

168 number with 30 μM stenoparib, measured by plaque assay and RT-qPCR, respectively, compared to untreated controls (t=7.982 and 12.82, P=0.0002 for both) (Fig. 4A and Fig. 4B).

170 **Identifying effects of stenoparib on the coronavirus lifecycle.** Coronavirus inhibitors may target one or several intracellular growth stages, including virus entry (camostat mesylate,
172 hydroxychloroquine), endosomal processing (hydroxychloroquine, rapamycin), translation and RNA processing (lopinavir), and transcription and replication (remdesivir) (1, 11, 29). By
174 altering the time of addition (TOA) and duration of treatment *in vitro*, we can discern whether a drug affects virus entry, intracellular growth, or both. TOA experiments were conducted using
176 the viral plaque assay with NL63 as a surrogate for SARS-CoV-2, and RT-qPCR was performed in parallel to measure viral loads. We used remdesivir as a reference inhibitor, since its
178 mechanism, target and dosage range are known (30). Experiments to determine the lifecycle stages affected by stenoparib were performed as follows: a) to ascertain the effect on virus entry,
180 cells were transiently exposed to compounds starting 1 h before infection, and ending 1 h after infection; b) for effects on post-entry events, including transcription, processing, translation or
182 replication, compounds were added 1 h after infection, when a number of virions would have already entered cells, and treatment was continued until the experimental endpoint at 120 h; c) to
184 examine the maximum achievable effect of the compounds, a full-time assay was performed. Treatment was initiated simultaneously with virus infection and continued until the 120 h
186 endpoint (see Methods for a detailed description).

As shown in Fig. 5A, the antiviral activity of stenoparib is most notable when added post-
188 infection. The 60 μM stenoparib dose achieved complete inhibition of NL63 plaquing, with no detectable (N/D) plaques following post-entry treatment compared to untreated cells ($P<0.0001$).
190 This is on par with the effect of 4 μM remdesivir, which also eliminated plaque formation. Likewise, assay results for the full-time treatment were comparable between stenoparib and
192 remdesivir, with 88.4% reduction in plaque efficiency for stenoparib ($t=5.582$, $P=0.0051$), and

full inhibition for remdesivir vs. untreated cells. This is consistent with results from RT-qPCR,
194 where stenoparib produced 98.7% (t=9.988, P=0.0099) and 95.5% (t=9.663, P=0.0105)
inhibition vs. untreated controls for post-entry and full-time drug exposure, also comparable to
196 the activity of remdesivir. These data are in line with those reported previously for the CVL218
PARP inhibitor and remdesivir (15).

198 With the plaque assay, we noticed a 16.5% reduction in plaque formation following
transient treatment with stenoparib early in the infection time course (i.e. "Entry"; Fig. 5A). This
200 effect was not markedly different than the results recorded for remdesivir (-27.8%; t=1.919,
P=0.1275). Inhibition of virus entry is not expected for remdesivir since its activity is specific to
202 blocking of RNA replication (30, 31), which is a mid-late event in the viral lifecycle. In contrast,
the results of RT-qPCR strongly support a specific effect for stenoparib on inhibiting virus entry,
204 where a 37.9% reduction in viral load is observed in the entry assay compared to just a 3.1%
reduction for remdesivir (t=4.352, P=0.0121) (Fig. 5B). Effects on viral entry are consistent with
206 the predicted activity of stenoparib on processes involved in early coronavirus infection events
(see Discussion). Taken as a whole, these observations suggest that stenoparib may affect
208 multiple targets that play roles in the early and late stages of coronavirus intracellular
multiplication.

210 **The combination of stenoparib and remdesivir strongly inhibits NL63.** Combination
drug therapies are widely used for the treatment for some of the worst human diseases, including
212 cancer (32), HIV/AIDS (33), and multidrug-resistant tuberculosis (34). The strategy of
combination therapy seeks to increase the beneficial effects of multiple drugs, lower their doses
214 to reduce adverse effects, and minimize the induction of resistance (35). Generally, the activity
of a drug combination is considered additive when the combined effect of two drugs is

216 equivalent to their individual doses, while if the effect is less than additive, the combination is considered antagonistic. Synergy occurs when the combined effect is greater than the additive
218 effect (35). Combinations of two or more drugs may lead to a synergistic effect by combining different mechanisms of action (MOA). Examples of synergistic combinations of drugs with
220 distinct MOAs include streptomycin–penicillin (36), trimethoprim–sulfa drugs (Co-trimoxazole) (37), and β-lactam/β-lactamase inhibitor combinations such as amoxicillin-clavulanate (38)
222 against bacterial infections.

Based on the fact that stenoparib and remdesivir inhibit coronavirus by distinct MOAs
224 (30, 31, 39), we approximated the half maximal effective concentration (EC_{50}) of stenoparib and remdesivir as 25.5 μM and 0.46 μM with NL63 and plaque assays. Calculations were aided by
226 the online calculator from AAT Bioquest ("Quest Graph™ EC50 Calculator." *AAT Bioquest, Inc*, 26 Oct. 2020, https://www.aatbio.com/tools/ec50-calculator). We hypothesized that a
228 combination of stenoparib and remdesivir would be more potent than the individual compounds. To explore this, we combined a range of doses of stenoparib with 0.5 μM remdesivir and tested
230 these for activity against NL63.

As shown in Fig. 6, complete inhibition of NL63 plaque formation was achieved with 60
232 μM stenoparib, in line with our earlier results with SARS-CoV-2 and Calu-3 cells (Fig. 3). Complete inhibition was also achieved with 1.0 μM remdesivir. However, a combination of 10
234 μM stenoparib and 0.5 μM remdesivir was more effective than either compound alone at these doses, achieving 90.7% inhibition for the combination, vs. 18.5% inhibition for 10 μM
236 stenoparib, and 65.6% for 0.5 μM remdesivir, suggesting at least additive effects when the drugs are combined. Notably, the stenoparib dose (10 μM) used in the combination is far below the

238 compound's EC_{50} of 25.5 μM. Altogether, these results support investigating the use of stenoparib and remdesivir as a combinatorial therapy for SARS-family coronavirus infections.

240

Discussion

242 Prior to the emergence of COVID-19, attempts to identify inhibitors of coronavirus were mainly focused on SARS- and MERS-CoVs. The recent efforts to develop COVID-19
244 therapeutics runs the gamut from new drug discovery to repurposing existing drugs. There are some excellent reviews on the subject (17, 40). Here, we focus on the compound stenoparib,
246 formerly known as 2X-121, an inhibitor of the cellular enzyme PARP-1/2. Stenoparib is thought to inhibit SARS-CoV-2 by multiple mechanisms, predominately by inhibiting of ADP-
248 ribosylation of proteins required for virus replication and assembly (41). ADP-ribosylation is a conserved, post-translational modification that is key for proper formation of the coronavirus
250 nucleocapsid, and inhibition can negatively affect packaging of the viral genome and virion stability. Specific targets of ADP-ribosylation include viral nsp3 protein, which is essential for
252 virulence and a component of the replication/transcription complex (RTC) (42, 43). Moreover, PARP inhibitors may exert additional protective effects at the host and cellular levels by
254 reducing depletion of NAD+ and ATP that leads to cell necrosis (39), as well as decreasing the pro-inflammatory NF-kB-triggered cytokine storm that can damage host organs (44). It has also
256 been suggested that PARP inhibitors enhance the degradation of the host type I interferon receptor (IFN-1R), which would also have a modulatory effect on the host inflammatory
258 response (45).

In this study, inhibition of SARS-family coronaviruses by stenoparib *in vitro* is likely due
260 to interference with multiple virus lifecycle events. Consistent with its predicted mechanism, stenoparib is effective when introduced post-infection. Additionally, we noted an association
262 between stenoparib treatment and decreased virus counts soon after infection. This may reflect activity against multiple targets, including those involved in promoting virus entry. Stenoparib

264 interference with the activity of tankyrase and Wnt/β-catenin signaling can affect expression of
the ACE2 receptor, leading to a decrease in the number of viruses that can enter the cell, which is
266 consistent with effects on virus entry and with our observations. In contrast, inhibition by
remdesivir was predominately on post-entry events. The effect of remdesivir on virus entry was
268 minimal, at best, which is in line with its specific targeting of the virus replication machinery.
Overall, our observations imply multiple mechanisms for stenoparib, including impeding of viral
270 entry and intracellular growth via modifications of multiple viral and host proteins. This is in
contrast to many current therapeutics that affect a narrow set of virus lifecycle events.

272 Other human coronaviruses that utilize ACE2 for binding and entry may be suitable as
surrogate platforms for the study of SARS-CoV-2 *in vitro,* so long as they can be propagated in
274 the laboratory and are able to elicit cellular infection phenotypes that can be quantitatively
measured. We show that the human seasonal coronavirus NL63, which can cause a cold-like
276 illness in humans (25), is such an example. Like SARS-CoV-2 and SARS-CoV, NL63 is
internalized following the binding of viral S-complex proteins to the ACE2 receptor (27, 46-48).
278 According to our observations, NL63 is susceptible to inhibition by compounds that affect
SARS-CoV-2, including remdesivir, the protease inhibitors camostat mesylate and E64d, and
280 stenoparib, the subject of this study.

In light of the *in vitro* cytotoxic effects of stenoparib, we were unable to test it against
282 SARS-CoV-2 at doses exceeding 30 μM in Vero E6 cells. Stenoparib was developed as a
cytotoxic drug for cancer treatment (14), so it is not surprising that it showed dose-dependent
284 cytotoxicity against rapidly-dividing Vero E6 cells. PARP inhibitors typically express their
lethality after several replication cycles (49). Thus, the susceptibility of Vero E6 cells to
286 stenoparib toxicity may be linked to its fast-growing phenotype, since two replication cycles can

be achieved in as little as 48 h. Although LLC-MK2 cells, which are utilized for propagation and
288 testing of NL63 are substantially more resistant to stenoparib, their susceptibility to SARS-CoV-
2 infection is suboptimal. We were thus presented with a conundrum in how to test high doses of
290 stenoparib against SARS-CoV-2 to assess its maximum activity. This was addressed through the
use of the Calu-3 human lung carcinoma cell line. Our results confirm the suitability of Calu-3 as
292 a host for SARS-CoV-2 and its high degree of resistance to stenoparib toxicity. This
characteristic of Calu-3 cells was predicted *in silico* using a method previously employed on
294 clinical tumor biopsies (21) and experimentally validated in this study. Infection of Calu-3
monolayers with SARS-CoV-2 formed large, clearly visible plaques, and in this regard, the
296 performance of Calu-3 surpassed Vero E6. A notable characteristic of Calu-3 is its slow growth
properties, which may coincide with a general degree of resistance to compounds that target
298 essential cellular pathways and are toxic to more rapidly dividing cells.

A promising drug to emerge from COVID therapeutic trials is the nucleoside analog
300 remdesivir, which shows activity against phylogenetically diverse viruses including Ebola,
Nipah, respiratory syncytial virus (RSV), and coronaviruses such as SARS- and MERS-CoV
302 (50), SARS-CoV-2 (30) and, as reported in this study, the seasonal human HCoV-NL63.
Reviews on the MOA of remdesivir have been published (17, 40, 50). After entering the cell,
304 remdesivir is triple phosphorylated to form remdesivir-triphosphate, and this structure is thought
to inhibit RNA polymerase, resulting in chain termination. While the precise molecular
306 mechanism is not clear (50), the EC_{50} of remdesivir has been reported to be 0.77 μM for SARS-
CoV-2 (30), which is in line with our measurement of 0.54 μM for SARS-CoV-2, and
308 comparable to our experimentally-determined EC_{50} of 0.46 μM against NL63.

While remdesivir inhibits the viral replicon, our data support multiple targets for
310 stenoparib. Moreover, our data support the efficacy of stenoparib and remdesivir as a potent
combination that is highly effective at inhibiting SARS-family coronaviruses inside cells. A
312 mixture of 10 μM stenoparib and 0.5 μM remdesivir was more successful at inhibiting the NL63
virus than either compound alone at these doses. Considering their distinct mechanisms and high
314 potency, a combination of remdesivir and stenoparib is likely to produce a synergistic effect on
additional SARS-family coronaviruses, including SARS-CoV-2. Studies involving this
316 combination in susceptible COVID-19 animal models are in line for efficacy testing.

318

Materials and Methods

320 The antiviral activity of stenoparib against coronaviruses was assessed *in vitro* using novel coronavirus SARS-CoV-2 isolate USA-WA1/2020 (deposited by the Centers for Disease
322 Control and Prevention and obtained through BEI Resources, NIAID, NIH: SARS-Related Coronavirus 2, Isolate USA-WA1/2020, NR-52281) and human coronavirus strain HCoV_NL63
324 (obtained through BEI Resources, NIAID, NIH: Human Coronavirus, NL63, NR-470). We used Vero E6 (ATCC® CRL-1586™) and Calu-3 cells (ATCC® HTB-55™) purchased from the
326 American Type Culture Collection (ATCC, Manassas, VA, USA) and maintained in EMEM (Eagle's Minimum Essential Medium) cell culture media (cat # 30-2003, ATCC, Manassas, VA,
328 USA) supplemented with 2% or 10% fetal bovine serum (FBS), 100 U/mL penicillin, 100 µg/mL streptomycin, 0.01 M HEPES buffer solution, 1 mM sodium pyruvate, 1x non-essential amino
330 acids solution (cat # SH3023801, Thermo Fisher Scientific, Waltham, MA, USA), and 2 mM L-glutamine for the propagation and experimentation with SARS-CoV-2. LLC-MK2 cells
332 (ATCC® CCL-7™) were maintained in Medium 199 (cat # M4530, Millipore Sigma, St. Louis, MO, USA) supplemented with 2% or 10% FBS, 100 U/mL penicillin, and 100 µg/mL
334 streptomycin, were used for the propagation and experimentation with the NL63 coronavirus. Inhibition of viral replication was assessed using reverse-transcription quantitative real-time PCR
336 (RT-qPCR) to measure the number of virions released into the cellular supernatant of infected cells and viral plaque formation assays (hereafter plaque assays), which measure a reduction in
338 plaque forming units (PFUs). Cytotoxicity was measured using Promega™ CytoTox 96™ Nonradioactive Cytotoxicity Assay (cat # G1780, Promega, Madison, WI, USA).

340 **Plaque assays.** 6-well plates (cat # CLS3516, Millipore Sigma, St. Louis, MO, USA) were seeded with ~3.0x10^5 cells/well and incubated for 48-72 h at 37°C in 5% CO2

342 atmosphere until 80-90% confluency was achieved, except for Calu-3 cells, which were incubated for >10 days to achieve 80-90% confluency. Prior to infection the 10% FBS
344 containing growth media was replaced with fresh media containing 2% FBS supplemented with varying concentrations of stenoparib as appropriate for each experiment (see results) and infected
346 with coronavirus (SARS-CoV-2 or NL63) at an MOI of 0.013 for SARs-CoV-2 and 0.003 for NL63 and incubated at 37°C for 1 h. The virus and drug containing media was then replaced
348 with a 1x DMEM (cat # D2902, Millipore Sigma, St. Louis, MO, USA) agarose overlay containing the appropriate drug concentration for each experiment, left to solidify at room
350 temperature for 15 minutes, and incubated for 120 h at 37°C in 5% CO2 atmosphere. Combined camostat mesylate and E64d (C/E) was used as an inhibition control for all experiments (20) and
352 all SARS-CoV-2 processes were conducted in a biosafety level 3 facility. After the 120 h incubation, 2 ml of 4% paraformaldehyde was added to each overlay and left to incubate for 30
354 minutes at room temperature to fix the cells and inactivate the virus. The cells were then stained with 1% crystal violet, the overlay was removed, and the cells were washed 3x with PBS. Plaque
356 forming units for each treatment group were counted, averaged, and normalized to the untreated control group. Each experimental run contained three biological replicates and each experiment
358 was conducted a minimum of two times. Standard deviation was calculated using the variation of averaged counts among all runs. Values were plotted using GraphPad Prism version 8.0.0 for
360 Windows (GraphPad Software, San Diego, CA, USA) and annotations were added using Adobe Illustrator (Adobe Systems Incorporated, San Jose, CA, USA). Where appropriate, statistical
362 significance was determined using a parametric unpaired t-test in GraphPad Prism version 8.0.0.

RT-qPCR: Infection and viral RNA extraction. 12-well plates (cat # CLS3513,
364 Millipore Sigma, St. Louis, MO, USA) were seeded with ~1.0x10^5 cells/well and incubated for

48-72 h at 37°C in 5% CO2 atmosphere until 80-90% confluency was achieved, except for Calu-
366 3 cells which were incubated for >10 days to achieve 80-90% confluency. Prior to infection the growth media was replaced with fresh media containing 2% FBS supplemented with varying
368 concentrations of stenoparib as appropriate for each experiment (see results) and infected with coronavirus (SARS-CoV-2 or NL63) at an MOI of 0.04 for SARs-CoV-2 and 0.01 for NL63 and
370 incubated for up to 120 h at 37°C in 5% CO2 atmosphere. C/E was used as an inhibition control for all experiments and all SARS-CoV-2 processes were conducted in a biosafety lab level 3
372 facility. Each experimental run contained two biological replicates and each experiment was conducted three times. 400 µL of supernatant was harvested at 48 h for SARS-CoV-2 but 120 h
374 for NL63 and RNA was extracted using Invitrogen Pure-Link RNA kits (Thermo Fisher Scientific, Waltham, MA, USA) following the manufacturer's recommendations for liquid
376 extractions.

RT-qPCR: Signature identification and qPCR assay design. Two TaqMan qPCR
378 assays were designed to target and amplify either the SARS-CoV-2 or the NL63 coronavirus. For NL63, the reference genome (NC_005831) was sliced into 200 nucleotide fragments,
380 overlapping by 20 nucleotides, resulting in 1,368 regions. These fragments were aligned against a set of 2,771 coronavirus genomes with blat v36.2 (51) in conjunction with LS-BSR v1.2.2 (52).
382 Regions were identified that had a blast score ratio (BSR) (53) value ≥0.8 in 60 NL63 genomes and a BSR value <0.4 in all other coronavirus genomes. A total of 10 fragments were identified
384 that were highly specific to all NL63 genomes based on these criteria. Primers and probes were identified from all fragments using Primer3 v2.3.6 (54) and regions that failed to align with non-
386 target coronavirus genomes were identified. A similar process was conducted for SARS-CoV-2 assay design, except the GCF_009858895.2 reference genome was used to generate 1,486

388 potential assay fragments. A total of 4 fragments were identified that were unique to 64 SARS-CoV-2 genomes. A probe was designed to a unique fragment in the spike protein targeting the
390 furin cleavage site with Primer3. Primers were designed from flanking regions.

The SARS-CoV-2 qPCR amplified a 125 bp region of the spike protein (GenBank Gene
392 ID: 43740568) using forward primer CoV2-S_19F (5'-GCTGAACATGTCAACAACTC-3') and reverse primer CoV2-S_143R (5'-GCAATGATGGATTGACTAGC-3') with MGB TaqMan
394 probe CoV2-S_93FP (5'-ACTAATTCTCCTCGGCGGGC-3') labelled fluorescently with a FAM dye, which was designed based off the SARS-CoV-2 genome GCF_009858895.2
396 (GenBank Sequence ID: MN908947.3), while the NL63 qPCR amplified a 191 bp region of a membrane protein (GenBank Gene ID: YP_003770.1) using forward primer NL63_10F (5'-
398 TGGTCGCTCTGTTAATGAAA-3') and reverse primer NL63_200R (5'-AAATTTCTTCCTAGCAGCTC-3') with MGB TaqMan probe NL63_102RP (5'-
400 CCCTCCTGAGAGGCAACACC-3') fluorescently labelled with a VIC dye, which was based off the HCoV_NL63 genome (GenBank Sequence ID: MN306040.1).

402 **RT-qPCR: Reverse transcription and PCR amplification.** Two approaches were used over the course of this study for the reverse transcription of RNA into cDNA followed by qPCR.
404 For the first approach we used a two-step method where viral RNA was converted into cDNA using Invitrogen SuperScript IV VILO Master Mix (cat # 11766500, Thermo Fisher Scientific,
406 Waltham, MA, USA) in 96-well format according to the manufacturer's recommendations and deactivated using 1 µL of Invitrogen RNase H (cat # 18021-014, Thermo Fisher Scientific,
408 Waltham, MA, USA); these processes used a SimpliAmp® thermocycler (Applied Biosystems, Foster City, CA, USA). 1 µL of template cDNA was then subjected to qPCR in 10 µL reactions
410 containing 1x TaqMan Universal Master Mix II (w/o AmpERASE UNG) (Applied Biosystems,

Foster City, CA, USA), with 0.2 µM of each forward and reverse primer and 0.1 µM of probe for the SARS-CoV-2 qPCR and 0.25 µM of each forward and reverse primer and 0.125 µM of probe for the NL63 qPCR, and thermocycled in triplicate reactions using either a QuantStudio 7 flex or QuantStudio 12K (Applied Biosystems, Foster City, CA, USA) under the following conditions: 10 minutes at 95°C, proceeded by 40 cycles of 95°C for 15 seconds and 60°C for 1 minute. The second approach employed a one-step procedure in which viral RNA was converted to cDNA using the TaqMan amplification primers, immediately followed by qPCR. For this approach we used the 4x Reliance One-Step Multiplex RT-qPCR Supermix (cat # 12010220, BioRad, Hercules, CA, USA) with the same TaqMan primers, probes, and concentrations as described above for the two-step approach; however, these reactions were conducted in 20 µL volumes, instead of 10 µL. Triplicate reactions were thermocycled using the same QuantStudio instruments described previously under the following conditions: 50°C for 10 minutes to reverse transcribe the viral RNA into cDNA, followed by 95°C for 10 minutes, proceeded by 40 cycles of 95°C for 10 seconds and 60°C for 30 seconds. Positive amplification and non-template controls were included on every run.

RT-qPCR: Data analysis. Synthetic double stranded DNA fragments were generated (gBlocks Gene Fragments, Integrated DNA Technologies, Coralville, IA, USA) as qPCR controls for both RT-qPCR assays. Both controls contained the amplification primers and internal gene sequence for either the SARS-CoV-2 or the NL63 target genes (see qPCR assay design section) and were elongated to 200 bp. These gBlocks were resuspended according to the manufacturer's protocol and quantified using a Qubit 4 fluorometer with a dsDNA HS assay kit (cat # Q32851 Thermo Fisher Scientific, Waltham, MA, USA) then normalized to 10^8 copies per µL using the calculated concentration and the molecular weight of each oligo. By making a

434 serial dilution of these gBlocks from 10^8 (undiluted) to 10^-1 copies and including them on every run, we were able to extrapolate viral copy number in each of the experimental samples.
436 Based on the inclusion of these predefined synthetic gBlock standards the QuantStudio instrument software generated a standard curve for each run that was used to quantify the
438 unknown sample reactions. The calculated quantities for triplicate reactions for each sample were averaged and the standard deviation was calculated among reactions. Values for the
440 experimental replicates and the standard deviations among experimental runs were averaged and then normalized to the untreated control group to obtain percent inhibition values. These values
442 were plotted using GraphPad Prism version 8.0.0 for Windows and annotations were added using Adobe Illustrator. Where appropriate, statistical significance was determined using a parametric
444 unpaired t-test in GraphPad Prism version 8.0.0.

Cytotoxicity. Cytotoxicity was measured using the Promega™ CytoTox 96™
446 Nonradioactive Cytotoxicity Assay kit (cat # G1780, Promega, Madison, WI, USA) in 50 µL reactions and 96-well format (cat # 161093, Thermo Fisher Scientific, Waltham, MA, USA)
448 according to the manufacturer's protocol, except we used 20 µL of 10X Lysis Solution per 100 µL of sample and incubated at 37°C for 30 minutes to generate the maximum LDH release
450 control. The assay was measured using a BioTeK Synergy™ HT plate reader (model # 7091000, BioTek, Winooski, VT, USA) at an optical density of 490 nm (OD_{490}). Cytotoxicity was
452 measured for ≤60 µM stenoparib for all three cell lines (LLC-MK2, Vero E6, and Calu-3). LLC-MK2 cells were assessed for cytotoxicity at 120 h, whereas Vero E6 and Calu-3 cells were
454 assessed for cytotoxicity every 24 h from 1-5 days. Percent cytotoxicity was calculated by dividing the experimental LDH release at OD_{490} by the maximum LDH release control at OD_{490}
456 and then multiplied by 100.

Time of addition experiments. For the full-time experiments, virus and drug compound
458 were incubated together for 1 h and then the media was replaced with fresh media containing the drug compound only. Entry experiments were pretreated with the drug compound for 1 h and
460 then infected with virus for an additional hour. The media was then replaced with fresh media containing no drug compound or virus. Post-entry experiments were infected with virus for 1 h.
462 The media was then replaced with fresh media containing the drug compound. Time of addition experiments were only conducted on the NL63 coronavirus. Statistical significance was
464 determined using a parametric unpaired t-test in GraphPad Prism version 8.0.0.

Stenoparib in combination with remdesivir. We performed plaque assays and used
466 these data to estimate the EC_{50} of stenoparib and remdesivir (cat # 329511, MedKoo Biosciences, Morrisville, NC, USA) against NL63 and SARS-CoV-2 (remdesivir only) in LLC-
468 MK2 and Vero E6 cells, as appropriate, using the results from at least two experimental runs. The EC_{50} values were approximated using the online calculator available from AAT Bioquest
470 ("Quest Graph™ EC50 Calculator." *AAT Bioquest, Inc*, 26 Oct. 2020, https://www.aatbio.com/tools/ec50-calculator).

472

Acknowledgments

474 This research was supported by a grant from The Flinn Foundation and continuing support of The Cowden Endowment for Microbiology. Core experiments were also supported by service
476 fees paid by Allarity Therapeutics.

478 **Conflict of Interest Statement**

SK is employed by and holds a financial interest in Allarity Therapeutics, which stands to potentially benefit from these results.

References

1. Hu B, Guo H, Zhou P, Shi ZL. 2020. Characteristics of SARS-CoV-2 and COVID-19. Nature Reviews Microbiology doi:10.1038/s41579-020-00459-7.
2. Wu ZY, McGoogan JM. 2020. Characteristics of and Important Lessons From the Coronavirus Disease 2019 (COVID-19) Outbreak in China Summary of a Report of 72 314 Cases From the Chinese Center for Disease Control and Prevention. Jama-Journal of the American Medical Association 323:1239-1242.
3. Liu Y, Mao B, Liang S, Yang JW, Lu HW, Chai YH, Wang L, Zhang L, Li QH, Zhao L, He Y, Gu XL, Ji XB, Li L, Jie ZJ, Li Q, Li XY, Lu HZ, Zhang WH, Song YL, Qu JM, Xu JF, Treatment SC. 2020. Association between age and clinical characteristics and outcomes of COVID-19. European Respiratory Journal 55.
4. Wu C, Chen X, Cai Y. 2020. Risk factors associated with acute respiratory distress syndrome and death in patients with coronavirus disease 2019 pneumonia in Wuhan, China (vol 180, pg 934, 2020). Jama Internal Medicine 180:1031-1031.
5. Guan W, Ni Z, Hu Y, Liang W, Ou C, He J, Liu L, Shan H, Lei C, Hui DSC, Du B, Li L, Zeng G, Yuen KY, Chen R, Tang C, Wang T, Chen P, Xiang J, Li S, Wang JL, Liang Z, Peng Y, Wei L, Liu Y, Hu YH, Peng P, Wang JM, Liu J, Chen Z, Li G, Zheng Z, Qiu S, Luo J, Ye C, Zhu S, Zhong N, Grp CMTE. 2020. Clinical Characteristics of Coronavirus Disease 2019 in China. New England Journal of Medicine 382:1708-1720.
6. Dong E, Du H, Gardner L. 2020. An interactive web-based dashboard to track COVID-19 in real time. Lancet Infect Dis 20:533-534.
7. Impact JHCfC. 2020. Coronavirus Resource Center - COVID Tracker. https://www.arcgis.com/apps/opsdashboard/index.html#/409af567637846e3b5d4182fcd779bea. Accessed
8. Team IC-F. 2020. Modeling COVID-19 scenarios for the United States. Nat Med doi:10.1038/s41591-020-1132-9.
9. Rabi FA, Al Zoubi MS, Kasasbeh GA, Salameh DM, Al-Nasser AD. 2020. SARS-CoV-2 and Coronavirus Disease 2019: What We Know So Far. Pathogens 9.
10. Hoffmann M, Kleine-Weber H, Schroeder S, Kruger N, Herrler T, Erichsen S, Schiergens TS, Herrler G, Wu NH, Nitsche A, Muller MA, Drosten C, Pohlmann S. 2020. SARS-CoV-2 Cell Entry Depends on ACE2 and TMPRSS2 and Is Blocked by a Clinically Proven Protease Inhibitor. Cell 181:271-280 e8.
11. Poduri R, Joshi G, Jagadeesh G. 2020. Drugs targeting various stages of the SARS-CoV-2 life cycle: Exploring promising drugs for the treatment of Covid-19. Cell Signal 74:109721.
12. Astuti I, Ysrafil. 2020. Severe Acute Respiratory Syndrome Coronavirus 2 (SARS-CoV-2): An overview of viral structure and host response. Diabetes Metab Syndr 14:407-412.
13. Dziadkowiec KN, Gasiorowska E, Nowak-Markwitz E, Jankowska A. 2016. PARP inhibitors: review of mechanisms of action and BRCA1/2 mutation targeting. Prz Menopauzalny 15:215-219.
14. McGonigle S, Chen ZH, Wu JY, Chang P, Kolber-Simonds D, Ackermann K, Twine NC, Shie JL, Miu JZT, Huang KC, Moniz GA, Nomoto K. 2015. E7449: A dual inhibitor of PARP1/2 and tankyrase1/2 inhibits growth of DNA repair deficient tumors and antagonizes Wnt signaling. Oncotarget 6:41307-41323.
15. Ge Y, Tian T, Huang S, Wan F, Li J, Li S, Yang H, Hong L, Wu N, Yuan E, Cheng L, Lei Y, Shu H, Feng X, Jiang Z, Chi Y, Guo X, Cui L, Xiao L, Li Z, Yang C, Miao Z, Tang H, Chen L, Zeng H, Zhao D, Zhu F, Shen X, Zeng J. 2020. A data-driven drug repositioning

framework discovered a potential therapeutic agent targeting COVID-19. bioRxiv doi:10.1101/2020.03.11.986836:2020.03.11.986836.
16. Pushpakom S, Iorio F, Eyers PA, Escott KJ, Hopper S, Wells A, Doig A, Guilliams T, Latimer J, McNamee C, Norris A, Sanseau P, Cavalla D, Pirmohamed M. 2018. Drug repurposing: progress, challenges and recommendations. Nat Rev Drug Discov doi:10.1038/nrd.2018.168.
17. Saha RP, Sharma AR, Singh MK, Samanta S, Bhakta S, Mandal S, Bhattacharya M, Lee SS, Chakraborty C. 2020. Repurposing Drugs, Ongoing Vaccine, and New Therapeutic Development Initiatives Against COVID-19. Front Pharmacol 11:1258.
18. Zhou YD, Hou Y, Shen JY, Huang Y, Martin W, Cheng FX. 2020. Network-based drug repurposing for novel coronavirus 2019-nCoV/SARS-CoV-2. Cell Discovery 6.
19. Qinfen Z, Jinming C, Xiaojun H, Huanying Z, Jicheng H, Ling F, Kunpeng L, Jingqiang Z. 2004. The life cycle of SARS coronavirus in Vero E6 cells. J Med Virol 73:332-7.
20. Li J, Zhan P, Liu X. 2020. Targeting the entry step of SARS-CoV-2: a promising therapeutic approach. Signal Transduct Target Ther 5:98.
21. Plummer R, Dua D, Cresti N, Drew Y, Stephens P, Foegh M, Knudsen S, Sachdev P, Mistry BM, Dixit V, McGonigle S, Hall N, Matijevic M, McGrath S, Sarker D. 2020. First-in-human study of the PARP/tankyrase inhibitor E7449 in patients with advanced solid tumours and evaluation of a novel drug-response predictor. Br J Cancer 123:525-533.
22. Chu H, Chan JF, Yuen TT, Shuai H, Yuan S, Wang Y, Hu B, Yip CC, Tsang JO, Huang X, Chai Y, Yang D, Hou Y, Chik KK, Zhang X, Fung AY, Tsoi HW, Cai JP, Chan WM, Ip JD, Chu AW, Zhou J, Lung DC, Kok KH, To KK, Tsang OT, Chan KH, Yuen KY. 2020. Comparative tropism, replication kinetics, and cell damage profiling of SARS-CoV-2 and SARS-CoV with implications for clinical manifestations, transmissibility, and laboratory studies of COVID-19: an observational study. Lancet Microbe 1:e14-e23.
23. Fogh J, Fogh JM, Orfeo T. 1977. One hundred and twenty-seven cultured human tumor cell lines producing tumors in nude mice. J Natl Cancer Inst 59:221-6.
24. Baer A, Kehn-Hall K. 2014. Viral concentration determination through plaque assays: using traditional and novel overlay systems. J Vis Exp doi:10.3791/52065:e52065.
25. van der Hoek L, Pyrc K, Berkhout B. 2006. Human coronavirus NL63, a new respiratory virus. FEMS Microbiol Rev 30:760-73.
26. Glowacka I, Bertram S, Herzog P, Pfefferle S, Steffen I, Muench MO, Simmons G, Hofmann H, Kuri T, Weber F, Eichler J, Drosten C, Pohlmann S. 2010. Differential downregulation of ACE2 by the spike proteins of severe acute respiratory syndrome coronavirus and human coronavirus NL63. J Virol 84:1198-205.
27. Li W, Sui J, Huang IC, Kuhn JH, Radoshitzky SR, Marasco WA, Choe H, Farzan M. 2007. The S proteins of human coronavirus NL63 and severe acute respiratory syndrome coronavirus bind overlapping regions of ACE2. Virology 367:367-74.
28. Schildgen O, Jebbink MF, de Vries M, Pyrc K, Dijkman R, Simon A, Muller A, Kupfer B, van der Hoek L. 2006. Identification of cell lines permissive for human coronavirus NL63. J Virol Methods 138:207-10.
29. Omarjee L, Janin A, Perrot F, Laviolle B, Meilhac O, Mahe G. 2020. Targeting T-cell senescence and cytokine storm with rapamycin to prevent severe progression in COVID-19. Clin Immunol 216:108464.
30. Wang M, Cao R, Zhang L, Yang X, Liu J, Xu M, Shi Z, Hu Z, Zhong W, Xiao G. 2020. Remdesivir and chloroquine effectively inhibit the recently emerged novel coronavirus (2019-nCoV) in vitro. Cell Res 30:269-271.
31. Chang CK, Jeyachandran S, Hu NJ, Liu CL, Lin SY, Wang YS, Chang YM, Hou MH. 2016. Structure-based virtual screening and experimental validation of the discovery of inhibitors targeted towards the human coronavirus nucleocapsid protein. Mol Biosyst 12:59-66.

582 32. Bigioni M, Benzo A, Irrissuto C, Lopez G, Curatella B, Maggi CA, Manzini S, Crea A, Caroli S, Cubadda F, Binaschi M. 2008. Antitumour effect of combination treatment with
584 Sabarubicin (MEN 10755) and cis-platin (DDP) in human lung tumour xenograft. Cancer Chemother Pharmacol 62:621-9.
586 33. Casado JL, Banon S. 2015. Dutrebis (lamivudine and raltegravir) for use in combination with other antiretroviral products for the treatment of HIV-1 infection. Expert Rev Clin
588 Pharmacol 8:709-18.
34. Caminero JA, Sotgiu G, Zumla A, Migliori GB. 2010. Best drug treatment for multidrug-
590 resistant and extensively drug-resistant tuberculosis. Lancet Infect Dis 10:621-9.
35. Garcia-Fuente A, Vazquez F, Vieitez JM, Garcia Alonso FJ, Martin JI, Ferrer J. 2018.
592 CISNE: An accurate description of dose-effect and synergism in combination therapies. Sci Rep 8:4964.
594 36. Reynolds B, Rowley D. 1953. Synergism between streptomycin and penicillin. British journal of experimental pathology 34:651-655.
596 37. Nichols RJ, Sen S, Choo YJ, Beltrao P, Zietek M, Chaba R, Lee S, Kazmierczak KM, Lee KJ, Wong A, Shales M, Lovett S, Winkler ME, Krogan NJ, Typas A, Gross CA.
598 2011. Phenotypic landscape of a bacterial cell. Cell 144:143-56.
38. Yogev R, Melick C, Kabat WJ. 1981. In vitro and in vivo synergism between amoxicillin
600 and clavulanic acid against ampicillin-resistant Haemophilus influenzae type b. Antimicrobial agents and chemotherapy 19:993-996.
602 39. Kouhpayeh S, Shariati L, Boshtam M, Rahimmanesh I, Mirian M, Zeinalian M, Salari-jazi A, Khanahmad N, Damavandi MS, Sadeghi P, Khanahmad H. 2020. The molecular story
604 of COVID-19; NAD+ depletion addresses all questions in this infection. preprint preprint doi:10.20944/preprints202003.0346.v1.
606 40. Pillaiyar T, Meenakshisundaram S, Manickam M. 2020. Recent discovery and development of inhibitors targeting coronaviruses. Drug Discov Today 25:668-688.
608 41. Grunewald ME, Fehr AR, Athmer J, Perlman S. 2018. The coronavirus nucleocapsid protein is ADP-ribosylated. Virology 517:62-68.
610 42. Lei J, Kusov Y, Hilgenfeld R. 2018. Nsp3 of coronaviruses: Structures and functions of a large multi-domain protein. Antiviral Res 149:58-74.
612 43. Fehr AR, Athmer J, Channappanavar R, Phillips JM, Meyerholz DK, Perlman S. 2015. The nsp3 macrodomain promotes virulence in mice with coronavirus-induced
614 encephalitis. J Virol 89:1523-36.
44. Gharote MA. 2020. Role of poly (ADP) ribose polymerase-1 inhibition by nicotinamide as
616 a possible additive treatment to modulate host immune response and prevention of cytokine storm in COVID-19. Indian Journal of Medical Sciences 72:25-28.
618 45. Coperchini F, Chiovato L, Croce L, Magri F, Rotondi M. 2020. The cytokine storm in COVID-19: An overview of the involvement of the chemokine/chemokine-receptor
620 system. Cytokine Growth Factor Rev 53:25-32.
46. Smith MK, Tusell S, Travanty EA, Berkhout B, van der Hoek L, Holmes KV. 2006.
622 Human angiotensin-converting enzyme 2 (ACE2) is a receptor for human respiratory coronavirus NL63. Adv Exp Med Biol 581:285-8.
624 47. Pohlmann S, Gramberg T, Wegele A, Pyrc K, van der Hoek L, Berkhout B, Hofmann H. 2006. Interaction between the spike protein of human coronavirus NL63 and its cellular
626 receptor ACE2. Adv Exp Med Biol 581:281-4.
48. Lin HX, Feng Y, Wong G, Wang L, Li B, Zhao X, Li Y, Smaill F, Zhang C. 2008.
628 Identification of residues in the receptor-binding domain (RBD) of the spike protein of human coronavirus NL63 that are critical for the RBD-ACE2 receptor interaction. J Gen
630 Virol 89:1015-1024.
49. Garnett MJ, Edelman EJ, Heidorn SJ, Greenman CD, Dastur A, Lau KW, Greninger P,
632 Thompson IR, Luo X, Soares J, Liu Q, Iorio F, Surdez D, Chen L, Milano RJ, Bignell GR,

Tam AT, Davies H, Stevenson JA, Barthorpe S, Lutz SR, Kogera F, Lawrence K, McLaren-Douglas A, Mitropoulos X, Mironenko T, Thi H, Richardson L, Zhou W, Jewitt F, Zhang T, O'Brien P, Boisvert JL, Price S, Hur W, Yang W, Deng X, Butler A, Choi HG, Chang JW, Baselga J, Stamenkovic I, Engelman JA, Sharma SV, Delattre O, Saez-Rodriguez J, Gray NS, Settleman J, Futreal PA, Haber DA, et al. 2012. Systematic identification of genomic markers of drug sensitivity in cancer cells. Nature 483:570-5.

50. Saha A, Sharma AR, Bhattacharya M, Sharma G, Lee SS, Chakraborty C. 2020. Probable Molecular Mechanism of Remdesivir for the Treatment of COVID-19: Need to Know More. Arch Med Res 51:585-586.

51. Kent WJ. 2002. BLAT--the BLAST-like alignment tool. Genome Res 12:656-64.

52. Sahl JW, Caporaso JG, Rasko DA, Keim P. 2014. The large-scale blast score ratio (LS-BSR) pipeline: a method to rapidly compare genetic content between bacterial genomes. PeerJ 2:e332.

53. Rasko DA, Myers GS, Ravel J. 2005. Visualization of comparative genomic analyses by BLAST score ratio. BMC Bioinformatics 6:2.

54. Rozen S, Skaletsky H. 2000. Primer3 on the WWW for general users and for biologist programmers. Methods Mol Biol 132:365-86.

Figures

654 **Fig. 1. Stenoparib exhibits dose-dependent inhibition of SARS-CoV-2 as measured by RT-**
qPCR. RT-qPCR was performed on viral RNA collected from cell culture supernatants at 48 h
656 post infection. Replicates within each run were averaged, and a total of three experiments were
performed. Error bars were based on averaged standard deviations within runs. Cytotoxicity
658 against Vero E6 cells was determined at 48 h using the Promega™ CytoTox 96™ assay kit, and
values represent the average of the two independent experiments (reported in Fig. 2A).
660

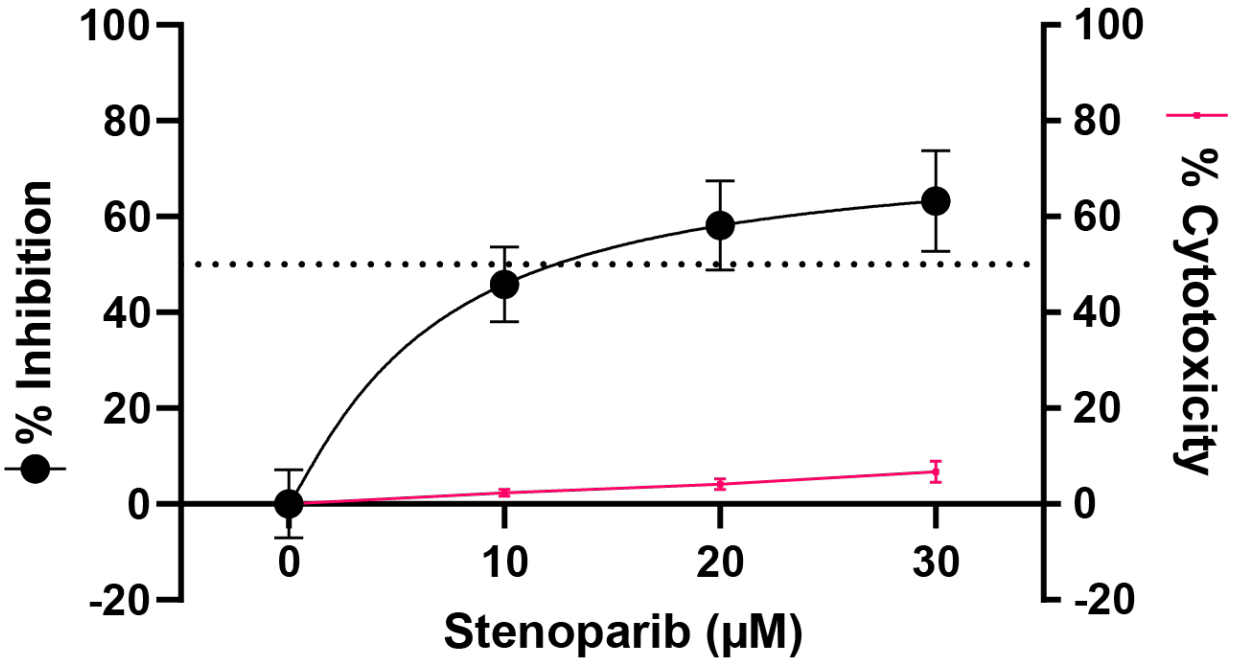

662

664 **Fig. 2. Stenoparib is cytotoxic in Vero E6 cells at concentrations greater than 30 µM, but not in Calu-3 cells.** Cytotoxicity was determined using the Promega™ CytoTox 96™ lactate-
666 dehydrogenase-release assay kit by harvesting culture media every 24 h up to 120 h post exposure. **A)** Vero E6 cells; **B)** Calu-3 cells, with 10, 20, 30, and 60 µM of stenoparib.
668 Measurements were normalized to cells treated with 1.0% Triton X-100 and compared to untreated controls. Biological replicates from two runs were averaged, and median values are
670 plotted. Results are representative of two experiments, and error bars are based on the standard deviation.

672

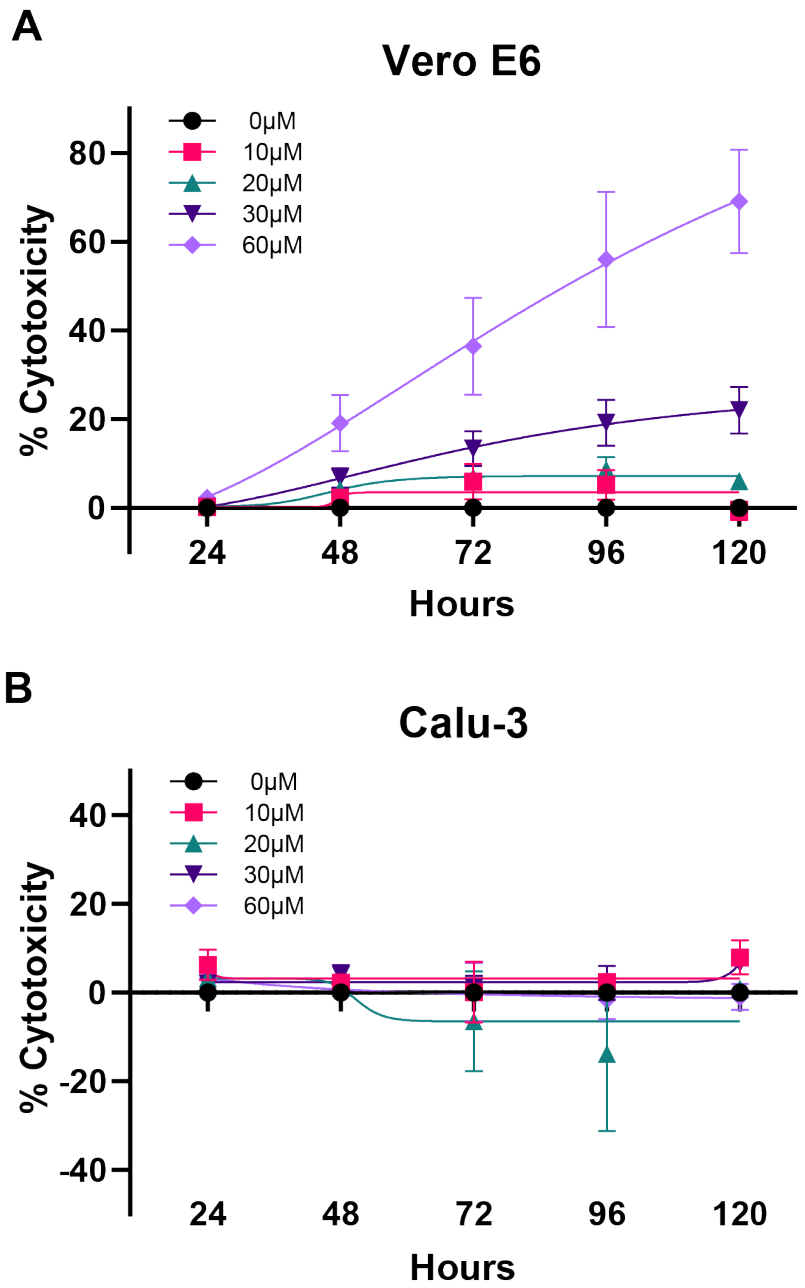

674 **Fig. 3. Stenoparib exhibits dose-dependent inhibition of SARS-CoV-2 in Calu-3 cells. A)**
Plaque forming efficiency using SARS-CoV-2. Values are normalized as a percentage of
676 inhibition compared to infected, but untreated cells. Plaques were counted 120 h after infection,
replicates from each run were averaged, and assays were performed three times. Error bars are
678 based on the standard deviation across all runs. **B)** RT-qPCR was performed on viral RNA
collected from cell culture supernatants at 48 h post infection and replicate values within each
680 run were averaged; a total of three runs were performed. Error bars are based on averaged
standard deviations within runs. Cytotoxicity against Calu-3 cells was determined at 48 and 120
682 h, as appropriate, using the Promega™ CytoTox 96™ assay kit, and values represent the average
of the two independent experiments (reported in Fig. 2B).

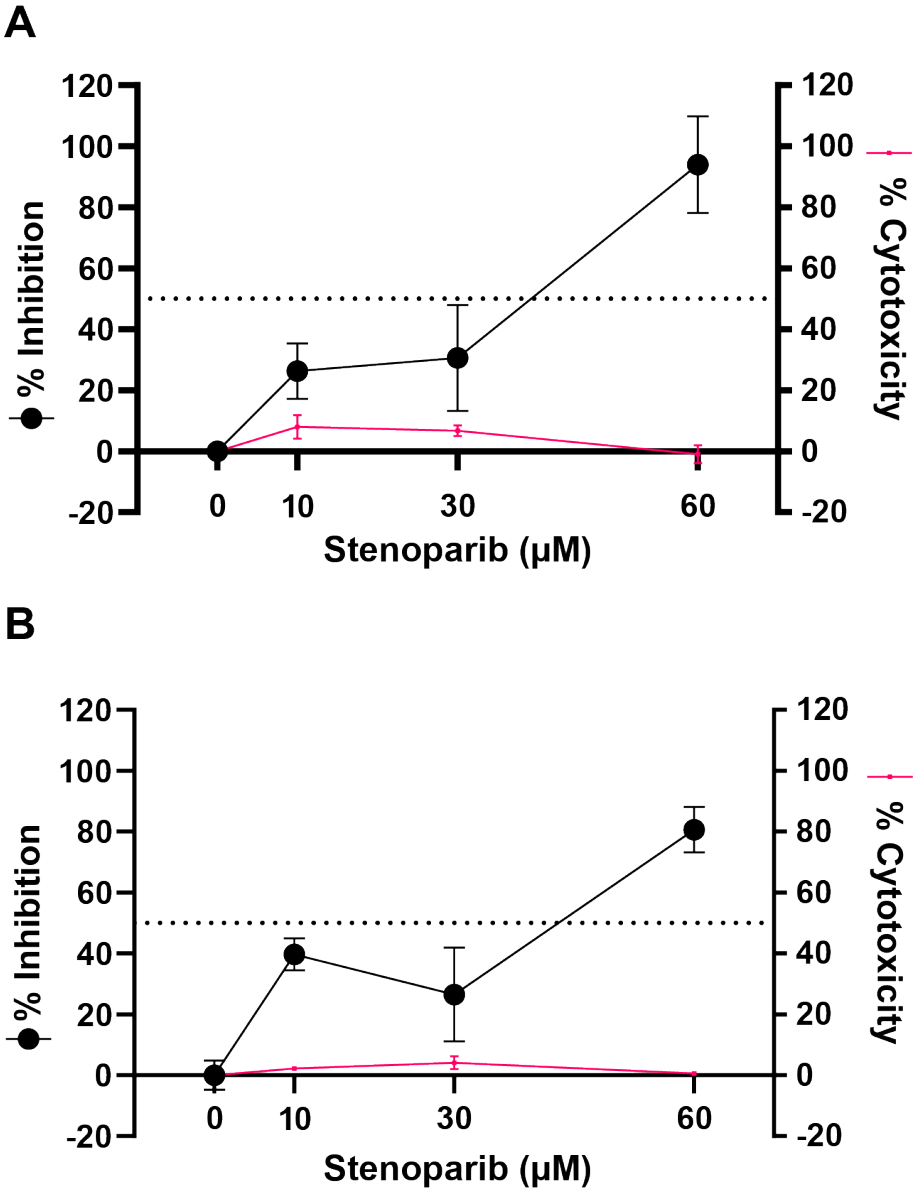

684

686

Fig. 4. Stenoparib exhibits dose-dependent inhibition of HCoV-NL63 in LLC-MK2 cells. A) Plaquing efficiency values are normalized as a percentage of inhibition compared to infected, but untreated cells. Plaques were counted 120 h after infection, and assays were performed three times. Error bars are based on the standard deviation across all runs. **B)** RT-qPCR was performed on viral RNA collected from cell culture media at 120 h post infection. Biological replicates from each run were averaged, and three independent runs were performed. Error bars were based on averaged standard deviations within runs. Cytotoxicity against LLC-MK2 cells was determined at 120 h using the Promega™ CytoTox 96™ assay kit, and values represent the average of the three independent experiments.

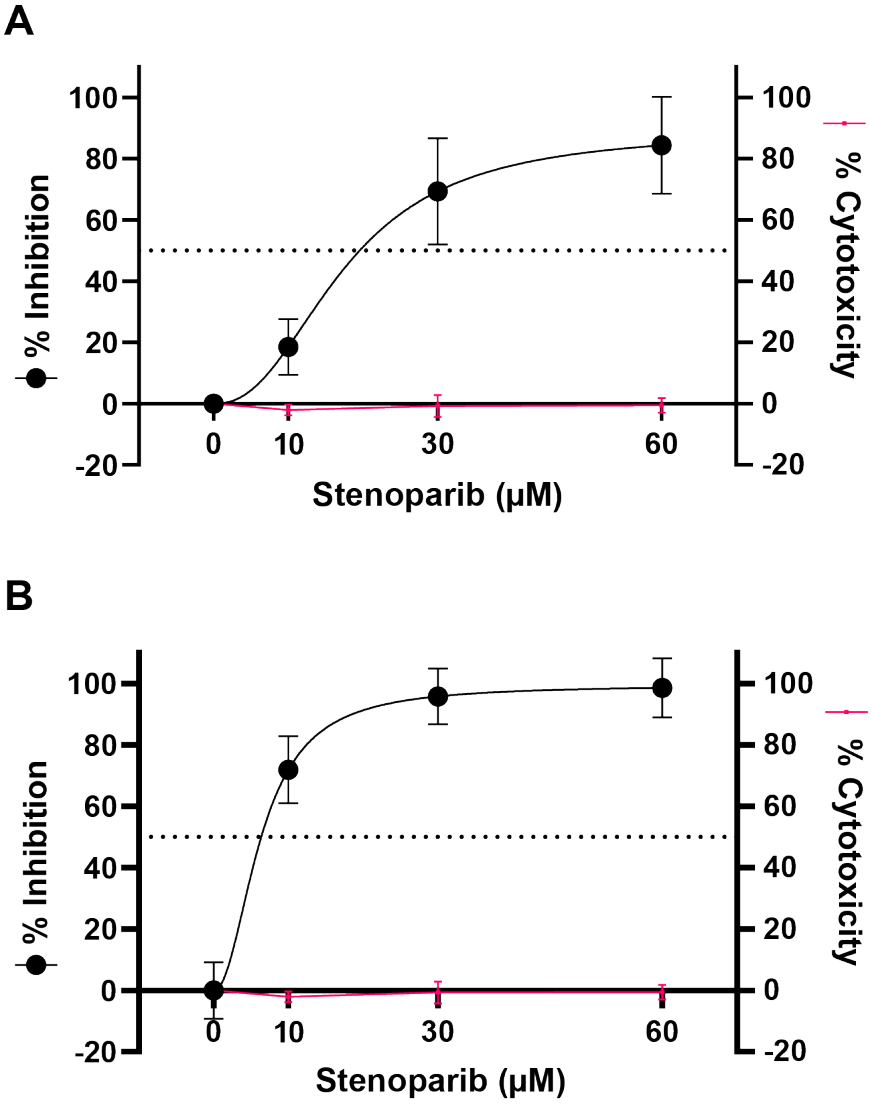

Fig. 5. Stenoparib inhibits HCoV-NL63 entry and post entry events while remdesivir inhibits post-entry. A) Plaque assays were performed three times and replicate plaque forming unit counts from each run were averaged. Error bars are based on standard deviation among runs. Brackets indicate the t-test comparison and P-value for the "Entry" group. No significant difference was observed between stenoparib and remdesivir under any treatment. N/D indicates that no plaques were detected in these treatment groups. **B)** RT-qPCR was performed on viral RNA collected from cell culture media at 120 h post infection and replicate values within each run were averaged; a total of three runs were performed. Error bars were based on averaged standard deviations within runs. Brackets indicate the t-test comparison and P-value for the "Entry" group. Significant differences were observed between stenoparib and remdesivir under all treatments.

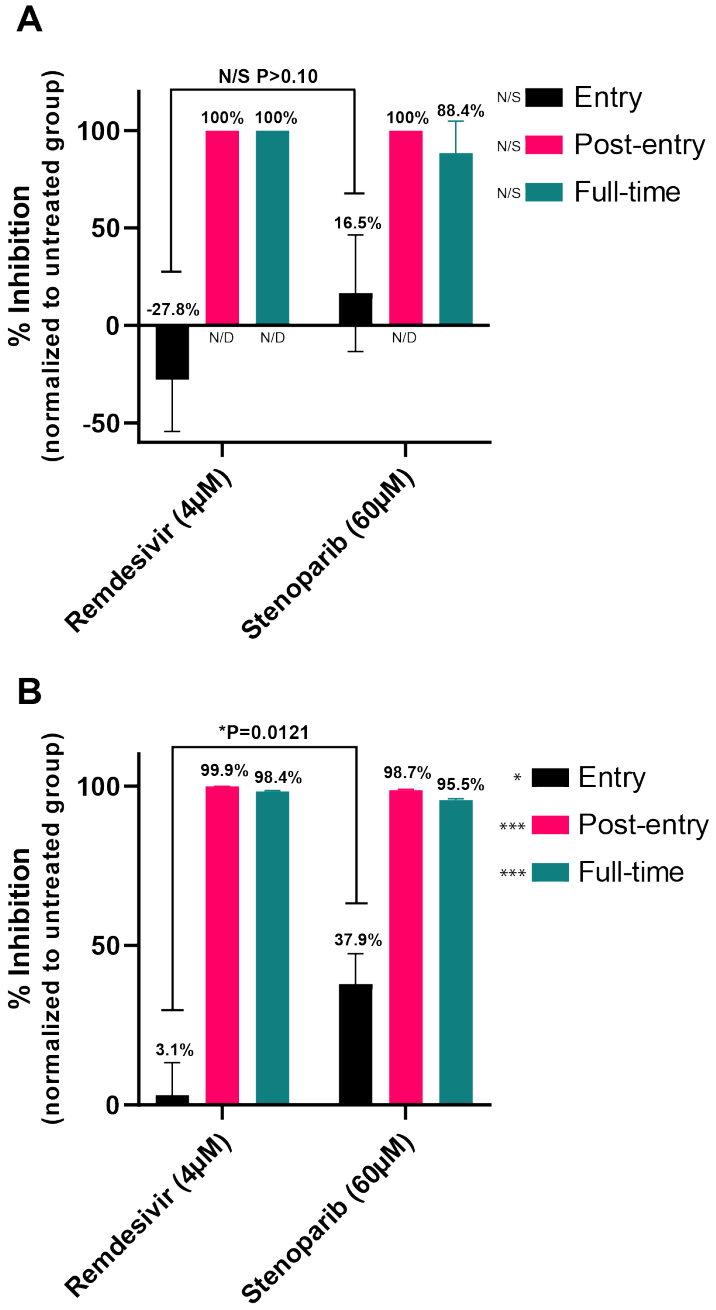

Fig. 6. Stenoparib and remdesivir in combination is a potent inhibitor of NL63. Plaque assays were performed a minimum of two times and replicate values from each run were averaged. Plaquing efficiency values are normalized as a percentage of inhibition compared to infected, but untreated cells. Three data sets are plotted to illustrate the treatment of NL63 with 1) stenoparib and 2) remdesivir as monotherapies and as a 3) combination therapy, whereby increasing concentrations of stenoparib are combined with 0.5 µM remdesivir; the EC_{50} was computationally approximated at 0.46 µM. The stenoparib monotherapy data is the same as previously reported (Fig. 4A). The synergistic activity threshold is defined as the sum of the mean values of 10 µM stenoparib and 0.5 µM remdesivir as monotherapies, while the grey highlighted area represents the minimum and maximum possible additive activity values based on the range of error for those same concentrations observed during these experiments.

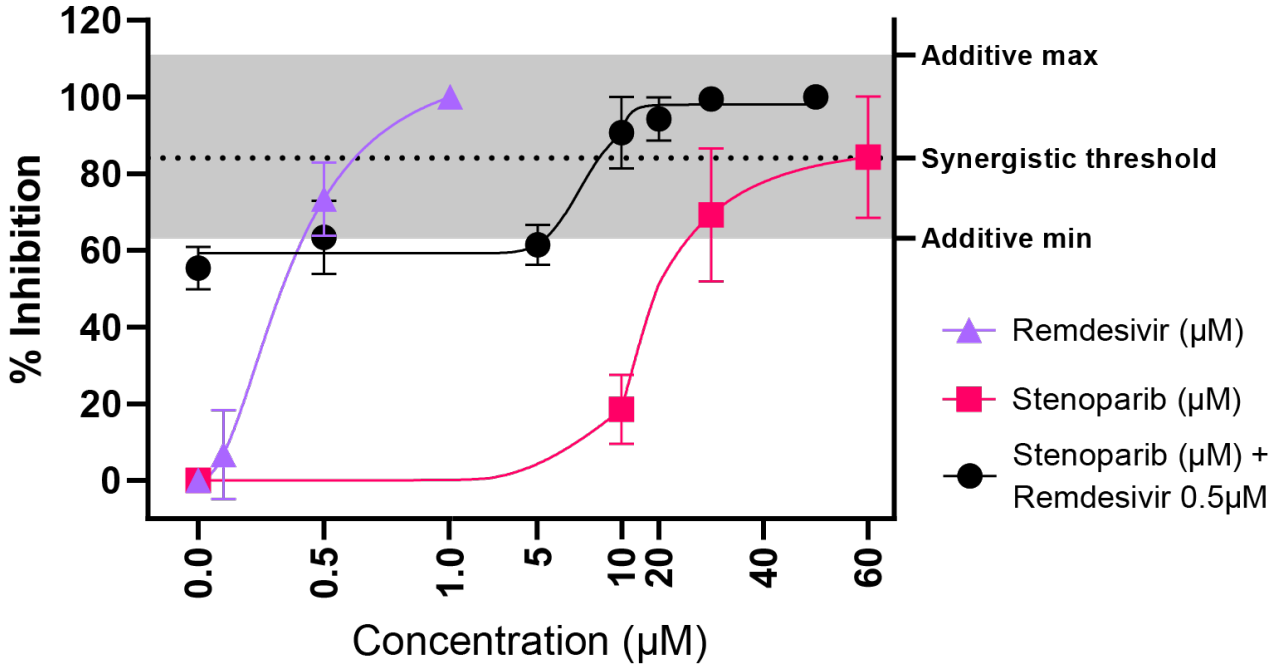
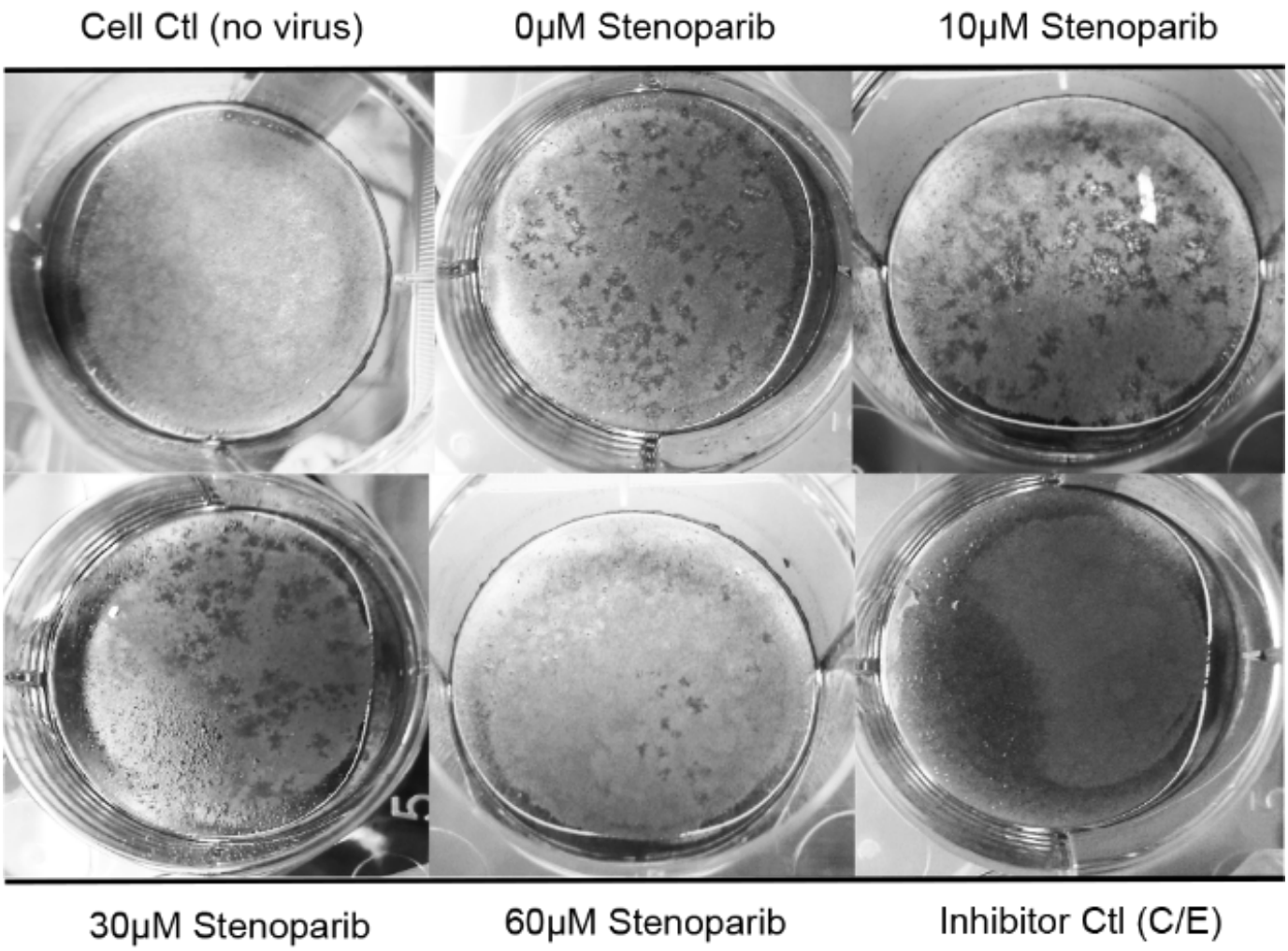
Fig. S1. Stenoparib inhibits plaque formation in Calu-3 cells. Plaque assays were performed using Calu-3 cells infected with SARS-CoV-2 and treated with varying concentrations of stenoparib. Plaques are identified as empty regions or "dead zones" in the cellular monolayer and are expressed as plaque forming units (PFUs) per well. Plaques were manually counted and averaged among experimental replicates. This score is normalized as a percentage of untreated, but infected cells. In this representative image of the SARS-CoV-2/Calu-3 experiment, plaques are dark scars on the cellular monolayer. Controls were 1) uninfected cells (Cell Ctl), 2) untreated, but infected cells (0 µM), and 3) a camostat mesylate and E64d (C/E) inhibitor control (Inhibitor Ctl). Treatment with stenoparib at 10 µM and 30 µM led to a marked reduction in plaquing efficiency, whereas 60 µM resulted in near complete inhibition.